

Computacional Analysis Of Potential Therapeutic Targets In The Inflammatory Pathway For Alcoholism

Mauricio Rey Buitrago^{1,2*} and Fabio Ancizar Aristizabal Gutierrez²

¹Faculty of Medicine, Universidad Nacional de Colombia, Bogotá, Colombia

²Department of Pharmacy, Universidad Nacional de Colombia, Bogotá, Colombia

*Corresponding autor at: Entrance Calle 53, building 426, Institute of Genetics, Universidad Nacional de Colombia, Bogotá, Colombia. E-mail address: mrey@unal.edu.co (Mauricio Rey).

Date of Submission: 04-12-2023

Date of Acceptance: 17-12-2023

ABSTRACT

Alcohol dependence is a multifactorial and polygenic disease, which, seeing it as an inflammatory condition, opens the possibility of exploring new diagnostic or monitoring biomarkers and new therapeutic agents to treat some of its harmful effects. In previous studies by our research group, two genes were discovered, through haplotype analysis, gene interactions and gene expression of the inflammatory response pathway: macrophage migration inhibitory factor (MIF) and α -synuclein (SNCA), which could be susceptible to therapeutic intervention. Using various bioinformatic tools, structural models for these two proteins were downloaded and built, validated and characterized. Promising ligand binding sites (drugs or drug candidates) were found and these interactions and the possible weak forces that would participate in this type of binding were modeled. In this work, two three-dimensional models were obtained for MIF, one model for SNCA, whose validation yielded reliable results. Potential binding sites with drugs or drug candidates, nine for MIF and one for SNCA, and their weak-type molecular interactions were identified.

Keywords: Inflammatory response, Therapeutic target, Alcohol, Protein modelling, Homology modelling, Molecular docking, *MIF*, *SNCA*

I. INTRODUCTION

Alcohol dependence is a multifactorial disease that has inflammatory properties. This opens the possibility of exploring new diagnostic or monitoring biomarkers and new therapeutic agents to treat some of its harmful effects [1,2]. Specific variants of genes related to this inflammatory response have been associated with the genetic risk

of alcohol addiction, and could become excellent therapeutic targets [3].

It is known that alcohol alters the levels of cytokines in various tissues. Its chronic and prolonged consumption promotes the production of proinflammatory cytokines and the inflammatory response, contributing to liver fibrosis and cirrhosis. After the liver, the brain is perhaps the most affected by chronic and abundant alcohol consumption, where the inflammatory response with long-term changes in behavior and neurodegeneration is clearly evident [4]. In previous work by our research group, a model that used the SNV-type markers of three genes: SCNA, IFNGR1 and MIF, as a single variable that better explained the results was suggested. The interaction between these three genes can be used as a risk prediction model to measure susceptibility to problematic alcohol consumption in the Colombian university population studied (5). However, when studying the gene expression of this same Colombian population, we observed downward changes in the form of mRNA for the TNFR1 and MIF genes in individuals with problematic alcohol consumption, while protein only decreased for MIF. In addition, the expression of SNCA, IL6R1 and MIF varied depending on the sex of the participants, specifically in men, downwards (6). Finally, we found that segments of the promoter of the SNCA and MIF genes were hypermethylated and that their expression was decreased in people who had problems with alcohol consumption. Considering the importance of characterizing these proteins, it is essential to perform bioinformatic analyzes to assess their role as potential therapeutic targets. In the past, the drug development process has been inefficient, costly, and has been based on trial-and-error testing of chemical compounds on cell cultures and/or laboratory animals. The paradigm has changed, and

currently, drug development requires the identification of a therapeutic target, a bioinformatics approach, and a large arsenal of computational tools (7).

Any approach to understanding how a protein works starts with studying its structure, and this depends on the order of the amino acid residues that make it up. The presence of chemical groups that determine the biological activity of the protein and its possible interaction with other molecules depends on its three-dimensional structure, which can be studied with different computer approaches. One strategy could be the design of drugs based on their three-dimensional structure, function analysis, and interactions. However, from the results obtained in the determination of three-dimensional structures of proteins, which have established that the protein structure is stable, the folding of all the proteins deposited in the database with 3D structure is in the range of 1,000 to 10,000, which means that models with good characteristics can be constructed (8,9).

Two proteins of interest, MIF and SNCA, were selected as potential drug targets after analyzing genetic variants, gene expression, and promoter methylation status. Using genetic, transcriptional, and methylation data, we identified and characterized two biomarkers, which could be potential therapeutic targets for alcoholism. They were modeled and characterized by us.

II. METHODOLOGY

Molecular docking was used to interact with the therapeutic target (protein) and the drug or drug candidate (ligand). The structure of the protein was searched in PDB (protein data bank, <https://www.rcsb.org/>), modeled in swissmodel (<https://swissmodel.expasy.org/>), model validation (<https://swissmodel.expasy.org/assess>) and the structure of the ligands were downloaded from drug bank (<https://go.drugbank.com/>). The search for MIF was limited to complete structures obtained by X-ray diffraction and from the human species. Only two structures presented good resolution and R values, were not mutants, and were not complexed with another compound. Meanwhile, for SNCA, limiting the search to the human species, a complete sequence, models obtained with good resolution X-rays, and 11 structures were obtained, although most were bound to a ligand and with not excellent resolution. The models found for SNCA were mutants, they formed clusters, and they were not of excellent quality. Therefore, this study was carried out in a mixed way, using models downloaded from the databases and by homology modeling, and then

docking. The interaction of a therapeutic target and various ligands was approached from a molecular perspective.

These protein sequences were searched in the Uniprot database (<https://www.uniprot.org/>), which is one of the most used protein sequence repositories in the world. The protein sequences were downloaded in FASTA format from there. The blast tool was used to compare the sequence of the white-unloaded proteins to those deposited in the PDB database and determine if they had a resolved crystallographic structure and their quality was evaluated. For one case, we then proceeded to build models by homology. The sequences of the proteins of interest were analyzed in the Swissmodel "modeller" program, where we obtained the templates. We selected some of them to generate our models. For both the MIF and SNCA, the models were selected and downloaded in PDB format, and then validated in pdbsum, verify3D, ProSa-web, and Quick2D.

In order to predict cavities in your 3D structures, the models were presented on the DoGSiteScorer platform (<https://proteins.plus/>) (10). The three-dimensional structures were observed with the pymol program (<https://pymol.org/>) and their interaction with the selected ligands was built with tools such as PATCHDOCK (<https://bioinfo3d.cs.tau.ac.il/PatchD>). From the Drugbank and/or Pubchem database, the ligands were selected, and their 3D structures were downloaded from there in pdb or other compatible format (8,11). Finally, the identification of non-covalent interactions between proteins and ligands with the selected site, considering the presence of water molecules, the protonation state of amino acid residues at physiological pH, and the delta G (free energy change of Gibbs) binding was done. This determination was made using the Protein-Ligand Interaction Profiler program (<https://plip-tool.biotec.tu-dresden.de/plip-web/plip/index>).

III. RESULTS

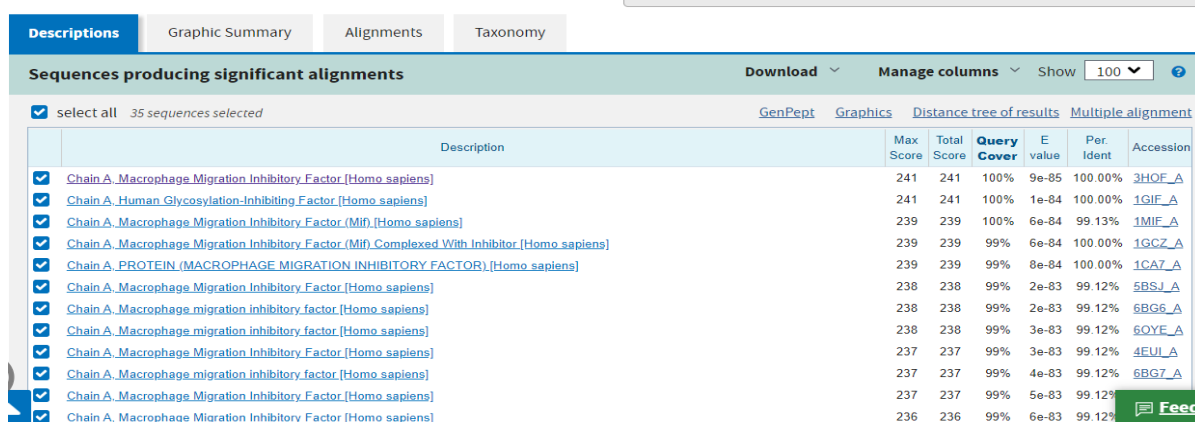
In the uniprot database, we searched for the sequence of the protein of interest (MIF), and we selected it and downloaded its sequence in FASTA format.

```
>sp|P14174|MIF_HUMAN Macrophage migration  
inhibitory factor OS=Homo sapiens OX=9606  
GN=MIF PE=1 SV=4  
MPMFIVNTNVPRASVPDGFSLSELTTQQLAQATG  
KPPQYIAVHVVPDQLMAFGGSSEPCALCSLHS  
IGKIGGAQNRYSKLLCGLLAERLRISPDRVYI  
NYYDMNAANVGWNNSTFA
```

We proceeded in the same way with the SNCA protein.

```
>sp|P37840|SYUA_HUMAN Alpha-synuclein
OS=Homo sapiens OX=9606 GN=SNCA PE=1
SV=1
MDVFMKGLSKAKEGVVAAAEEKTKQGVAEAA
GKTKEGVLYVGSKTKEGVVHGVATVAEKTKE
EQVTNVGGAVVTGVTAVAQKTVEGAGSIAA
ATGFVKKDQLGKNEEGAPQEGILEDMPVDPD
NEAYEMPSEEQYQDYEPEA
```

In BLAST, we aligned the sequences of interest against the PDB database. Alignment was performed between the amino acid residue sequences of the target proteins and the amino acid residues of the proteins deposited in the Protein Data database. BLAST server (12) uses the identity between amino acid sequences to determine the sequence identity. For MIF, two sequences deposited in the bank were found to have 100% identity, whereas for SNCA, only one was found to have 100% identity (12) (figure 1).



Descriptions | Graphic Summary | Alignments | Taxonomy

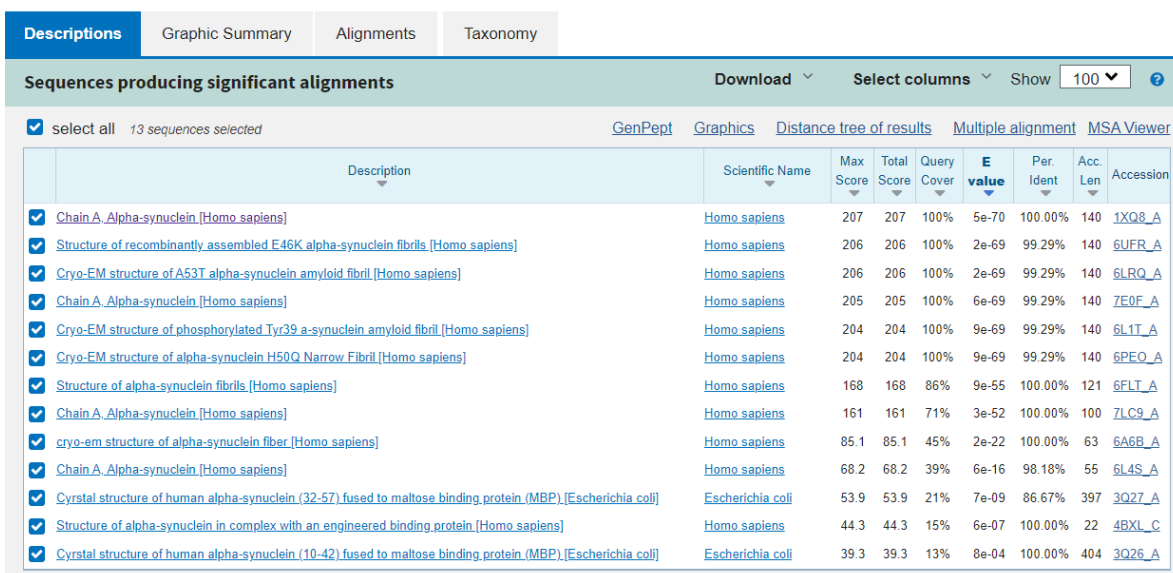
Sequences producing significant alignments

Download Manage columns Show 100

select all 35 sequences selected

| Description | Max Score | Total Score | Query Cover | E value | Per. Ident | Accession |
|--|-----------|-------------|-------------|---------|------------|-----------|
| Chain A_Macrophage Migration Inhibitory Factor [Homo sapiens] | 241 | 241 | 100% | 9e-85 | 100.00% | 3HOF_A |
| Chain A_Human Glycosylation-Inhibiting Factor [Homo sapiens] | 241 | 241 | 100% | 1e-84 | 100.00% | 1GIF_A |
| Chain A_Macrophage Migration Inhibitory Factor (Mif) [Homo sapiens] | 239 | 239 | 100% | 6e-84 | 99.13% | 1MIF_A |
| Chain A_Macrophage Migration Inhibitory Factor (Mif) Complexed With Inhibitor [Homo sapiens] | 239 | 239 | 99% | 6e-84 | 100.00% | 1GCZ_A |
| Chain A_PROTEIN (MACROPHAGE MIGRATION INHIBITORY FACTOR) [Homo sapiens] | 239 | 239 | 99% | 8e-84 | 100.00% | 1CAT_A |
| Chain A_Macrophage Migration Inhibitory Factor [Homo sapiens] | 238 | 238 | 99% | 2e-83 | 99.12% | 5BSJ_A |
| Chain A_Macrophage migration inhibitory factor [Homo sapiens] | 238 | 238 | 99% | 2e-83 | 99.12% | 6BG6_A |
| Chain A_Macrophage migration inhibitory factor [Homo sapiens] | 238 | 238 | 99% | 3e-83 | 99.12% | 6OYE_A |
| Chain A_Macrophage Migration Inhibitory Factor [Homo sapiens] | 237 | 237 | 99% | 3e-83 | 99.12% | 4EUL_A |
| Chain A_Macrophage migration inhibitory factor [Homo sapiens] | 237 | 237 | 99% | 4e-83 | 99.12% | 6BG7_A |
| Chain A_Macrophage Migration Inhibitory Factor [Homo sapiens] | 237 | 237 | 99% | 5e-83 | 99.12% | |
| Chain A_Macrophage Migration Inhibitory Factor [Homo sapiens] | 236 | 236 | 99% | 6e-83 | 99.12% | |

a)



Descriptions | Graphic Summary | Alignments | Taxonomy

Sequences producing significant alignments

Download Select columns Show 100

select all 13 sequences selected

| Description | Scientific Name | Max Score | Total Score | Query Cover | E value | Per. Ident | Acc. Len | Accession |
|--|------------------|-----------|-------------|-------------|---------|------------|----------|-----------|
| Chain A_Alpha-synuclein [Homo sapiens] | Homo sapiens | 207 | 207 | 100% | 5e-70 | 100.00% | 140 | 1XQ8_A |
| Structure of recombinantly assembled E46K alpha-synuclein fibrils [Homo sapiens] | Homo sapiens | 206 | 206 | 100% | 2e-69 | 99.29% | 140 | 6UFR_A |
| Cryo-EM structure of A53T alpha-synuclein amyloid fibril [Homo sapiens] | Homo sapiens | 206 | 206 | 100% | 2e-69 | 99.29% | 140 | 6LRQ_A |
| Chain A_Alpha-synuclein [Homo sapiens] | Homo sapiens | 205 | 205 | 100% | 6e-69 | 99.29% | 140 | 7E0F_A |
| Cryo-EM structure of phosphorylated Tyr39 alpha-synuclein amyloid fibril [Homo sapiens] | Homo sapiens | 204 | 204 | 100% | 9e-69 | 99.29% | 140 | 6LIT_A |
| Cryo-EM structure of alpha-synuclein H50Q Narrow Fibril [Homo sapiens] | Homo sapiens | 204 | 204 | 100% | 9e-69 | 99.29% | 140 | 6PEO_A |
| Structure of alpha-synuclein fibrils [Homo sapiens] | Homo sapiens | 168 | 168 | 86% | 9e-55 | 100.00% | 121 | 6FLT_A |
| Chain A_Alpha-synuclein [Homo sapiens] | Homo sapiens | 161 | 161 | 71% | 3e-52 | 100.00% | 100 | 7LC9_A |
| cryo-em structure of alpha-synuclein fiber [Homo sapiens] | Homo sapiens | 85.1 | 85.1 | 45% | 2e-22 | 100.00% | 63 | 6A6B_A |
| Chain A_Alpha-synuclein [Homo sapiens] | Homo sapiens | 68.2 | 68.2 | 39% | 6e-16 | 98.18% | 55 | 6L4S_A |
| Crystal structure of human alpha-synuclein (32-57) fused to maltose binding protein (MBP) [Escherichia coli] | Escherichia coli | 53.9 | 53.9 | 21% | 7e-09 | 86.67% | 397 | 3QZ7_A |
| Structure of alpha-synuclein in complex with an engineered binding protein [Homo sapiens] | Homo sapiens | 44.3 | 44.3 | 15% | 6e-07 | 100.00% | 22 | 4BXL_C |
| Crystal structure of human alpha-synuclein (10-42) fused to maltose binding protein (MBP) [Escherichia coli] | Escherichia coli | 39.3 | 39.3 | 13% | 8e-04 | 100.00% | 404 | 3QZ6_A |

b)

Figure 1 Alignment result of the sequence of interest MIF (a) and SNCA (b) with the sequences deposited in PDB.

Model generation

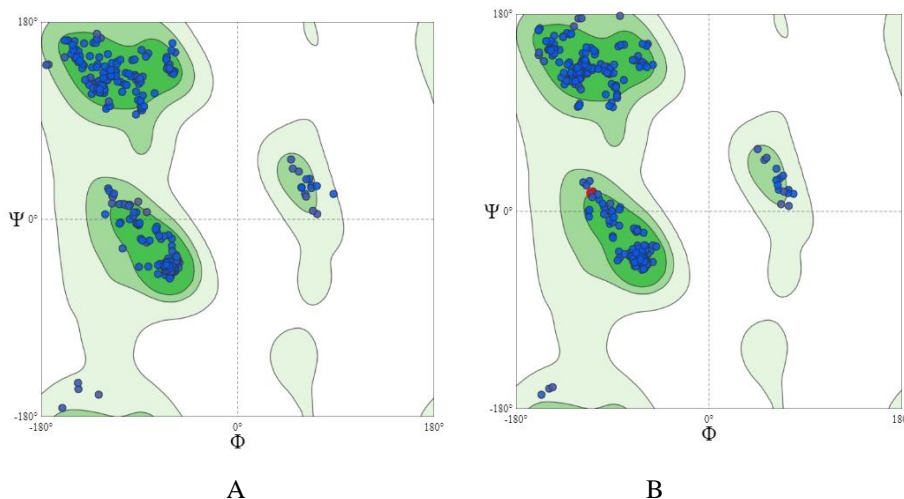
As previously mentioned, at PDB, we search for reported 3D structures using the following criteria: organism of origin, native or

mutant structure, method used to resolve it, degree of resolution, presence or absence of ligand, etc. We found structures, most of which were bound to ligands, some of which formed aggregates, with

highly varied values of validation criteria, from good to fair to bad to finally very bad. Both models were found in the database for both MIF and SNCA, with very varied quality parameters. It was decided to create models in Swiss model. We looked for templates to generate our models using the MODELLER program [11]. For MIF, 13 templates were found, all obtained by X-ray diffraction. Six of them had 100% identity, and nine of them were without ligands. Two templates (PDB codes: 1gif.1. A and 3dji.2.A) with GMQE values close to one were selected and with them two models were built, which we will call model 1 and model 2 from now on, respectively. For SNCA 9, templates were found, all with 100% identity, in addition to corresponding to the reference species. Seven of them were obtained by nuclear magnetic resonance (NMR), one by cryo-electron microscopy. Two templates were selected, the first from NMR (PDB code 2n0a.1). The second template, also NMR (PDB code 2n0a.1.b), with higher GMQE values, although low compared to the data for MIF. With them, two models were built that we will call model 1 and model 2, respectively.

Validation of models bio-informatically

For the two models of each protein, Ramachandran plots were obtained [12]. To validate the models, the Ramachandran graphs generated by the Swiss model structure assessment were used, which allows us to visualize the distribution of the dihedral angles psi and phi that contribute to the formation of the protein structure. The plots showed that most of the amino acid residues were found in favorable regions of MIF, with values of 98% and 96% for each model 1. Both models had a percentage of residues in unfavorable regions of approximately 0.30%. According to the standards, a model is of excellent quality when it has more than 90% of amino acid residues in the most favorable region (see Figure 3 a and b and Table 5-1). Our two models for MIF met this requirement. For the SNCA models, 91% and 88.41% of the amino acid residues were in favorable regions, the latter less than 90% to be considered of excellent quality and with higher values of residues in unfavorable regions. If we compare the two SNCA models with the models of the MIF protein, the two SNCA models are lower quality (see figure 2 and table 1).



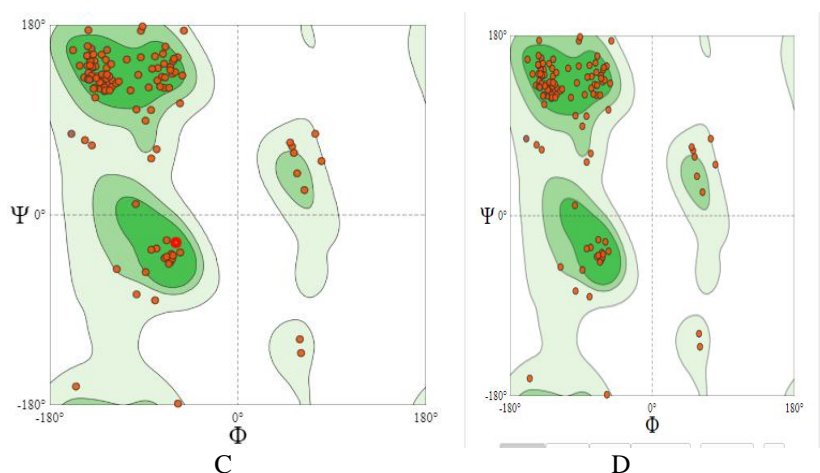


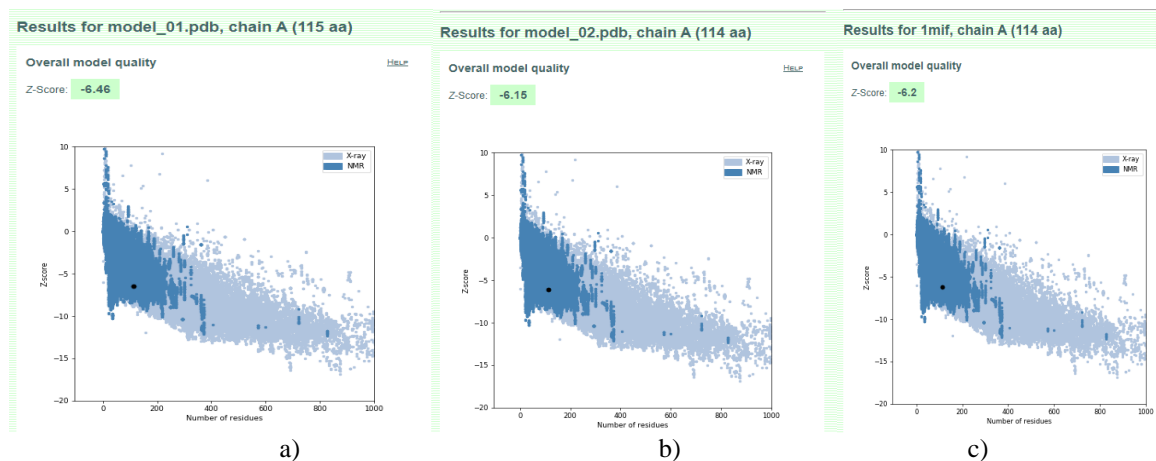
Figure 2 Results of Ramachandran plots for MIF, Model 1(A) and Model 2(B) and for SNCA, model 1(C) and model 2(D)

Table 1 Result of the parameters of the Ramachandran plots for the models obtained of the MIF protein (1 and 2) and of the SNCA protein (1 and 2)

| Characteristic Model | Residues (%) in favorable regions | Outliers (%) of residuals in allowed regions | Outliers (%) of residuals in unfavorable regions |
|-------------------------|-----------------------------------|--|--|
| MIF-Model 1 | 98.23 | 6,32 | 0,29 |
| MIF-Model 2 | 96.73 | 1,77 | 0.30 |
| SNCA-Model 1 | 91.30 | 1,45 | 0.97 |
| SNCA-Model 2 | 88.41 | 4,35 | 2.91 |

Zeta scores were also calculated on the ProSA Web server (<https://prosa.services.came.sbg.ac.at/prosa.php>) of the structures of the models obtained: for MIF, model 1 obtained a z value -6.46, while for model 2 it was -6.15, values close to the value obtained for the template protein (1MIF) which was -6.2. For

SNCA, the two models obtained a score of 1.37 further from the value obtained for the reference template protein, which was 1.8. The scores for MIF are within the characteristic range of the native protein, which means that the model structures do not contain errors. However, for SNCA, this indicator is not the best (see figure 3).



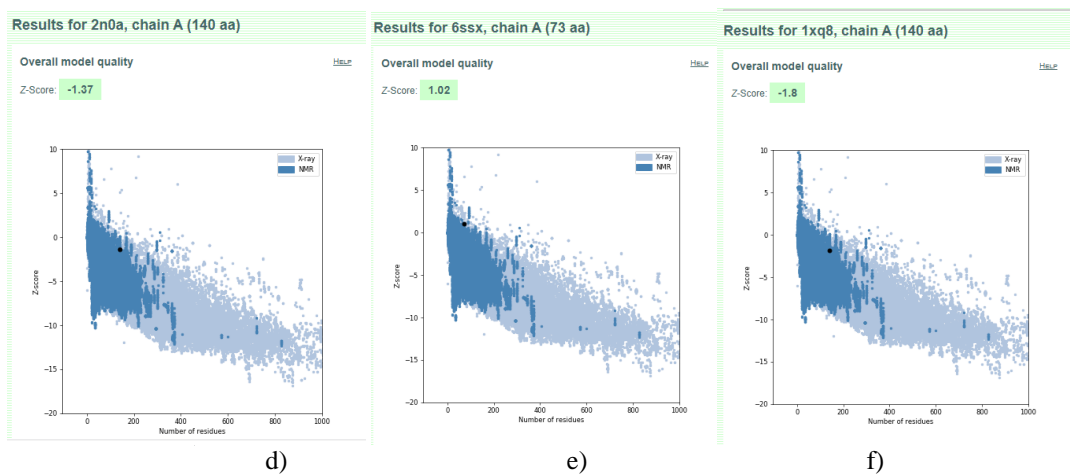
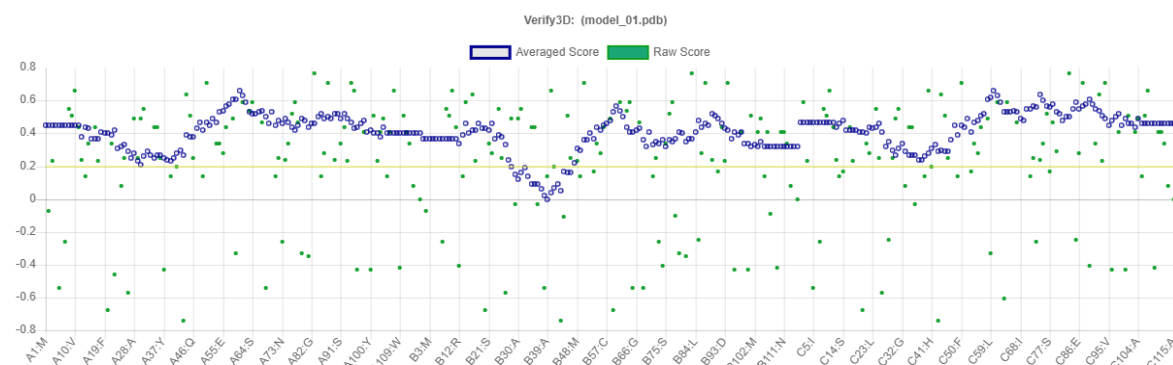
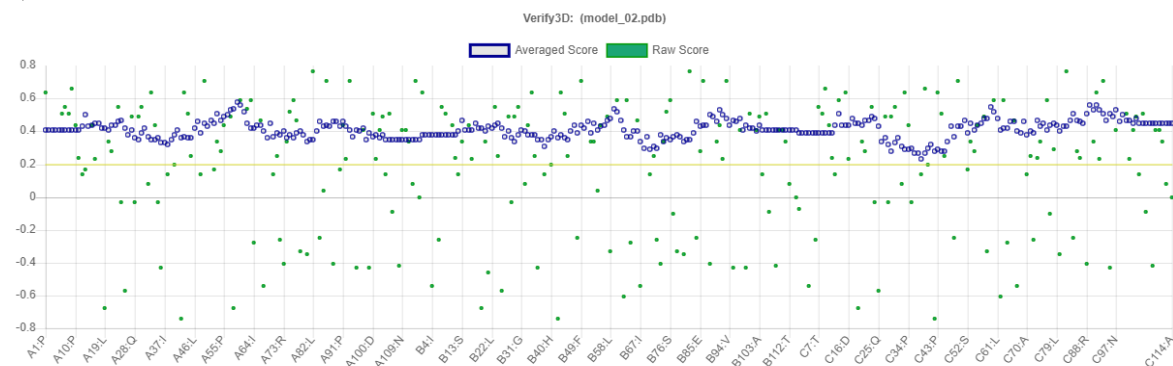


Figure 3 Results of the Z Values calculated with Web ProSa for MIF models 1, 2 and reference (a, b and c) and for SNCA models 1, 2 and reference (d, e and f)

The compatibility of the atomic model (3D) with its own amino acid sequence (1D) was analyzed with the Verify3D tool. The average 3D-1D score for model 1 of the MIF protein was equal to or greater than 0.2 for 94.78% of the amino acid residues. The analysis was thought to be successful. Furthermore, the program reports that at least 80% of the amino acid residues reached a score ≥ 0.2 in the 3D/1D profile (see figure 4).



a)



b)

Figure 4 3D-1D model compatibility for MIF model 1 (a) and model 2 (b).

However, for model 2, 100% of the amino acid residues reached an average score of 3D-1D ≥ 0.2 , passing the analysis. Furthermore, the program reports that at least 80% of the amino acid residues reached a score ≥ 0.2 in the 3D/1D profile (see figure 4). The results show that the two MIF models presented 1D-3D compatibility, with model 2 being the one with the best values, all higher than 0.2. But for the two SNCA models, the Verify3D tool returns an error and doesn't give any value.

Analysis of secondary structure and tertiary structure

After validation of the models, secondary structures were analyzed with the Quick2D tool (<https://toolkit.tuebingen.mpg.de/tools/quick2d>) [13]. The presence of two regions with alpha helices and four regions with beta folds is shown in the structures for MIF that have already been reported [12]. There are two regions of alpha helices and a region of beta folding observed in SNCA (see figure 5) [13,14].

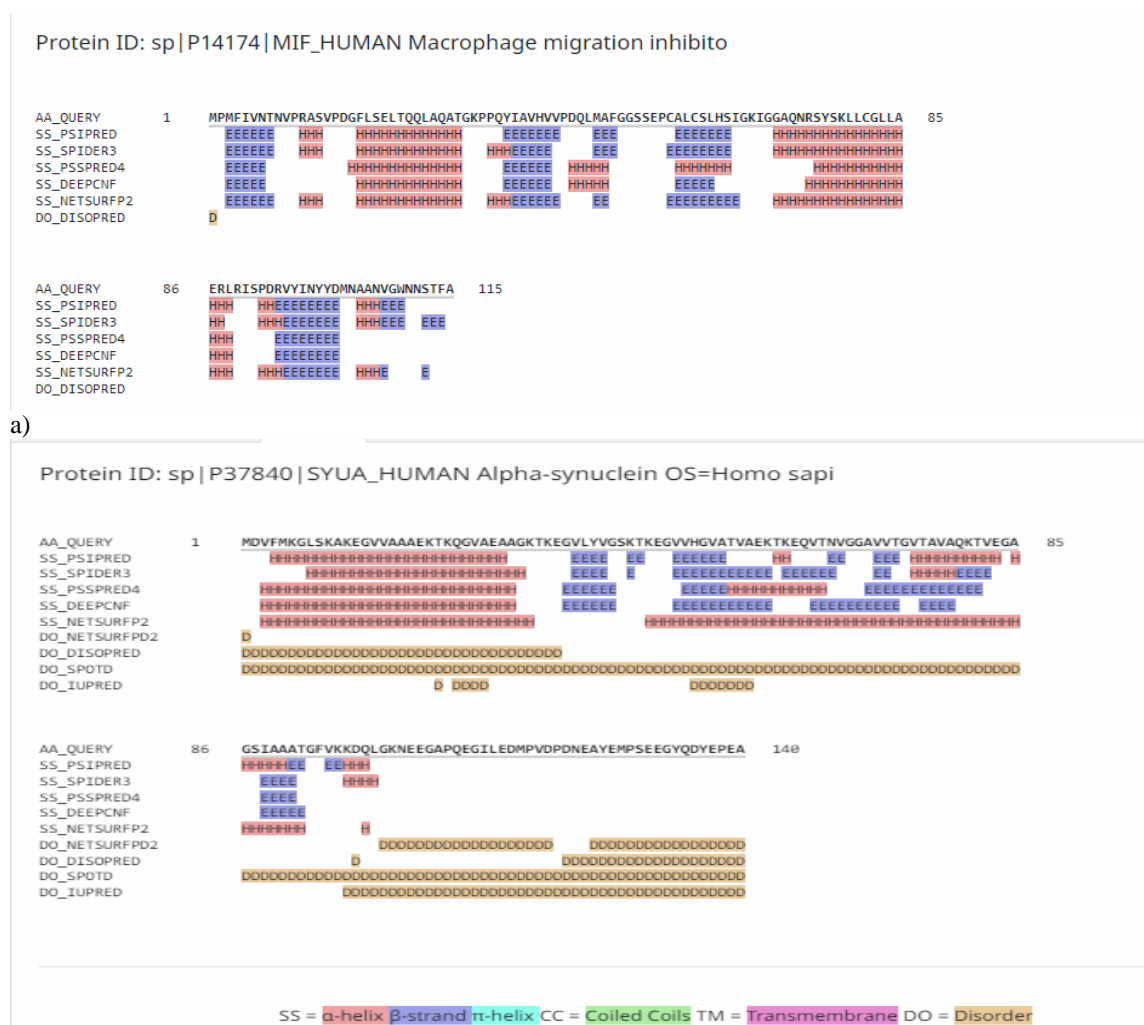


Figure 5 Secondary structures for the sequence of the selected proteins MIF (a) and SNCA (b)

When you look at the two three-dimensional models of MIF, you can see that they look very similar, with similar folded sheets and helix structures. We compared the models made by the Swiss prot program and found that most of the

residues had values of the LDDT indicator of one or close to one, with a global value of 0.9382. The models for SNCA show a global LDDT value of 0.3278 for model 1 and 0.3383 for model 2, which indicates that the models for this protein are poor.

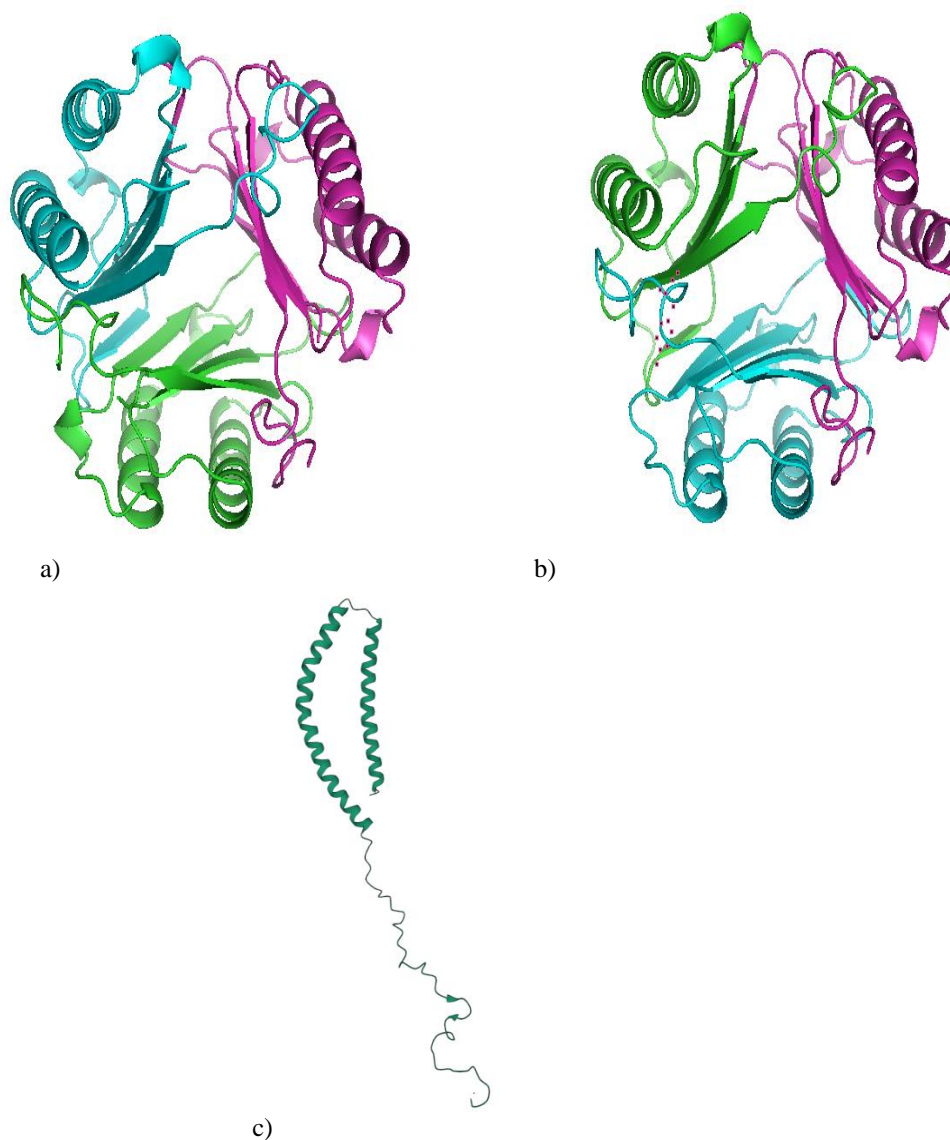


Figure 6 MIF model 1(a), model 2(b) obtained from swiss model server and SCNA model(c) downloaded from PDB and visualized with Pymol.

Analysis of cavities and interactions with ligands

Model 1 and 2 obtained in the Swiss model were downloaded in PDB format, visualized, and analyzed with PYMOL open source molecular viewer [15] open source molecular viewer (see figure 6). In addition, the prediction of cavities was found, which were presented on the DoGSiteScorer platform of proteinsplus (<https://poseview.zbh.uni-hamburg.de/> of proteinsplus), in which cavities were predicted in the 3D structure (see figure 7) and parameters of pharmacological interest were obtained [8]. Table 2 shows the most important parameters for cavities that could bind to different

ligands. The two MIF models had similar binding sites or cavities, which allowed binding or interaction with a ligand. This pocket was also present in the SNCA model. Afterward, the volume, area, and depth of the possible ligand binding sites were determined. The program provides a pharmacibility score by combining three parameters describing volume, hydrophobicity, and enclosure. In this manner, a cavity was established in each model with great interest for the binding of ligands, since it obtained high scores and much higher than the others.

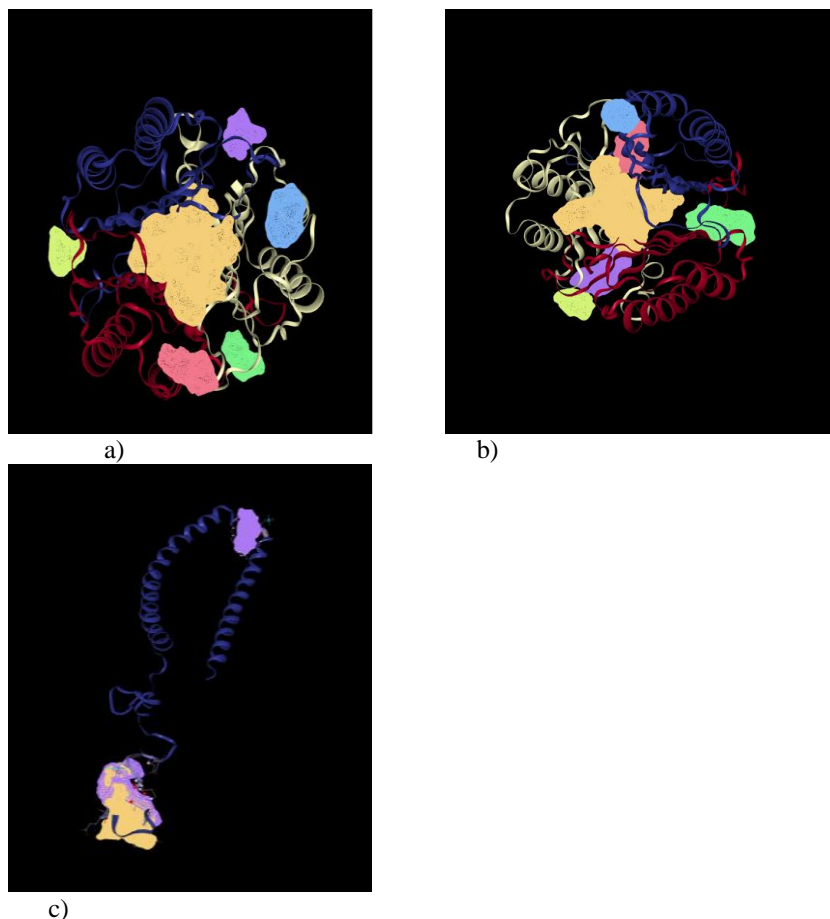


Figure 7 Detection of cavities, possible ligand binding sites for MIF model 1(a), model 2(b) and SNCA model (c)

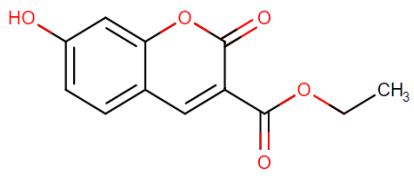
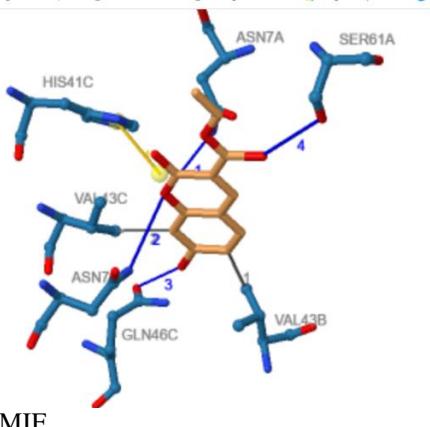
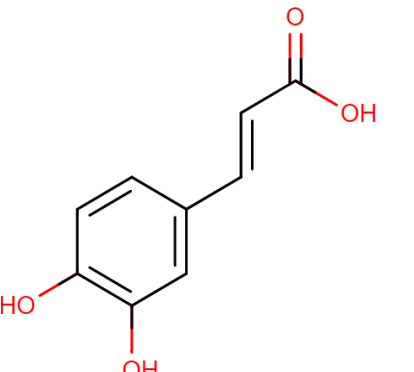
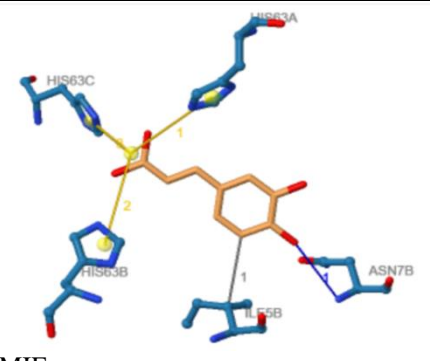
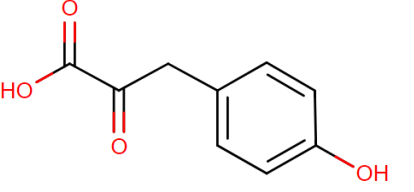
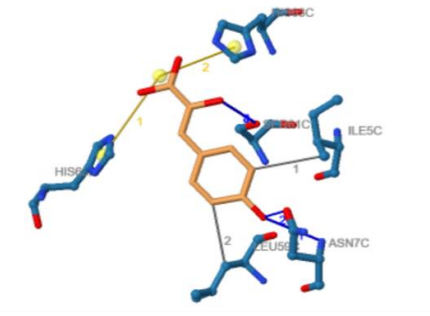
Table 2 Parameters of the detected cavities for the MIF model 1 and 2 and the SNCA model analyzed with program DoGSiteScorer and presented in figure 7

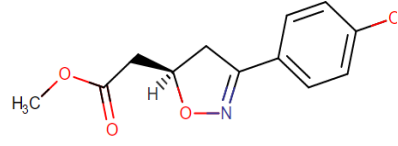
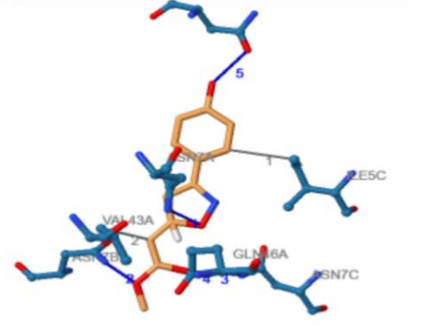
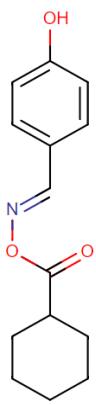
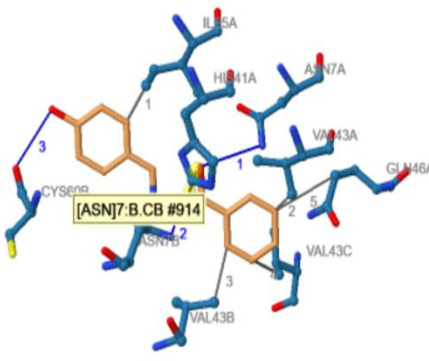
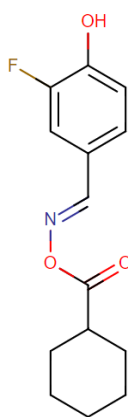
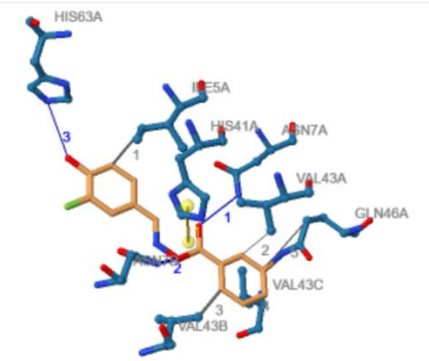
| Protein-Structure-Cavity | Volume | Area | Pharmacibility |
|--------------------------|----------------|----------------|----------------|
| MIF-Model 1-beige | 1569,79 | 1258,17 | 0,81 |
| MIF-Model 1-violet | 155,26 | 301,86 | 0,32 |
| MIF-Model 1-green | 149,12 | 341,53 | 0,25 |
| MIF-Model 1-pink | 147,71 | 367,41 | 0,39 |
| MIF-Model 1-blue | 133,18 | 292,99 | 0,25 |
| MIF-Model 1-lime green | 132,35 | 303,63 | 0,23 |
| MIF-Model 2-beige | 1337,02 | 1163,61 | 0,81 |
| MIF-Model 2- violet | 247,42 | 394,26 | 0,59 |
| MIF-Model 2- green | 217,28 | 298,41 | 0,51 |
| MIF-Model 2- pink | 198,91 | 257,07 | 0,41 |
| MIF-Model 2-blue | 112,77 | 259,96 | 0,25 |
| MIF-Model 2- lime green | 102,53 | 207,32 | 0,16 |
| SNCA-Model-yellow | 451,87 | 1167,42 | 0,72 |
| SNCA-Model-pink | 256,63 | 628,17 | 0,22 |

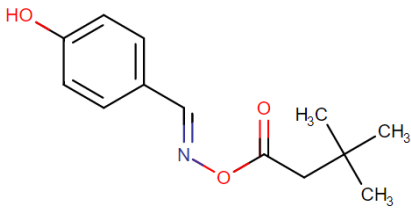
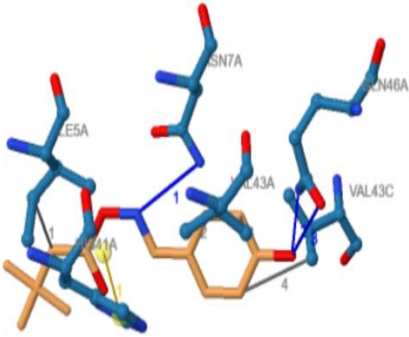
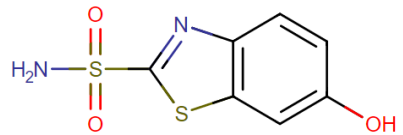
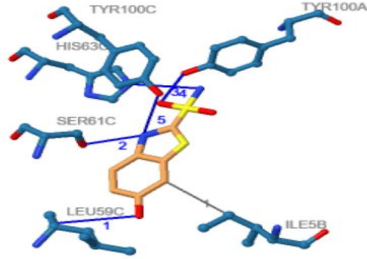
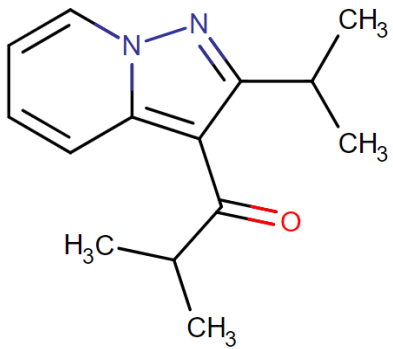
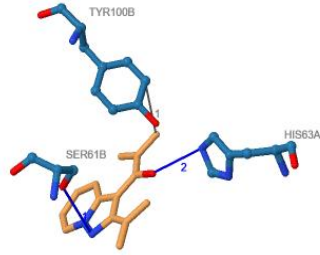
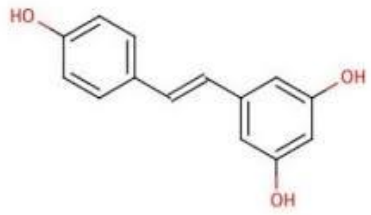
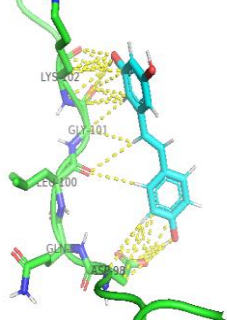
Then, we looked for ligands for the selected cavities. In the drug banks database, the products related to the proteins of interest (MIF and SNCA) were searched, which are listed below in Table 3. Then, an analysis of the interaction of model 2 MIF was conducted. The MIF protein and the selected ligand (drug or drug candidate, 9

structures) were docked using the PATCHDOCK and/or DOCKTHOR program. We identified non-covalent interactions between proteins and ligands using the Protein-Ligand Interaction Profiler program, available at <https://plip.biotec.tu-dresden.de/plip-web>.

Table 3 MIF ligands (homotrimer with A, B and C chains), 3D representation of the interaction of the binding site of MIF and various ligands and of SNCA with a single ligand.

| Ligand compound and protein interactions with coordinates | Structural formula of the ligand | Protein-ligand interaction |
|--|---|---|
| <p>7-Hydroxy-2-Oxo-Chromene-3-Carboxylic Acid Ethyl Ester</p> <p>Hydrophobic: 43B Val, 43C Val hydrogen bond: 7A Asn, 7C Asn, 46C Gln, 61A Ser Salt bridges: 41C His</p> |  |  <p>MIF</p> |
| <p>3,4-Dihydroxycinnamic Acid</p> <p>Hydrophobic: 5B Ile hydrogen bond: 7B Asn Salt bridges: 63A, 63B, 63C His</p> |  |  <p>MIF</p> |
| <p>4-Hydroxyphenylpyruvic acid (ENO)</p> <p>Hydrophobic: 5C Ile, 59C Leu hydrogen bond: 7C Asn, 7C Asn, 61 C Ser, 61C Ser Salt bridges: 63B and 63C His</p> |  |  <p>MIF</p> |

| | | |
|---|---|---|
| <p>3-(4-HYDROXYPHENYL)-4,5-DIHYDRO-5-ISOXAZOLE-ACETIC ACID METHYL ESTER</p> <p>Hydrophobic: 5C Ile, 43A Val hydrogen bond: 7A, Asn, 7B Asn, 7C Asn, 46A Gln, 98A Asn</p> |  |  <p>MIF</p> |
| <p>4-HYDROXYBENZALDEHYDE (CYCLOHEXYLCARBONYL)OXIME</p> <p>Hydrophobic: 5A Ile, 43A Val, 43B Val, 43C Val, 46A Gln Hydrogen bond: 7A Asn, 7B Asn, 60B Cys Salt bridges: 41A His</p> |  |  <p>MIF</p> |
| <p>3-FLUORO-4-HYDROXYBENZALDEHYDE (CYCLOHEXYLCARBONYL)OXIME</p> <p>Hydrophobic: 5A Ile, 43A val, 43B val, 43C val, 46A Gln hydrogen bond: 7A asn, 7B asn, 6 A his salt bridges: 41A his</p> |  |  <p>MIF</p> |

| | | |
|--|---|---|
| <p>4-HYDROXYBENZALDEHYDE O-(3,3-DIMETHYLBUTANOYL)OXIME</p> <p>Hydrophobic: 5A Ile, 43A Val, 43A Val, 43C Val hydrogen bond: 7A Asn, 46 A Gln, 46A Gln Salt bridges: 41 a His</p> |  |  <p>MIF</p> |
| <p>6-HYDROXY-1,3-BENZOTHAZOLE-2-SULFONAMIDE</p> <p>Hydrophobic: 5B Ile Hydrogen bond: 59C Leu 61C Ser, 63C His, 100A Tyr, 100C Tyr</p> |  |  <p>MIF</p> |
| <p>3-isobutryl-2-isopropylpyrazolo-[1,5-a]pyridine (ibudilast).</p> <p>Hydrophobic: Tyr 100B Hydrogen bond: Ser 61B Hydrogen bond: His 63A</p> |  |  <p>MIF</p> |
| <p>Resveratrol (3, 5, 4'-trihydroxi-trans-estilbeno)</p> <p>Hydrophobic: Leu100 Hydrogen bond: Asp98 Hydrogen bond: Gly101 Hydrogen bond: Lys102</p> |  |  <p>SNCA</p> |

IV. DISCUSSION OF RESULTS

We obtained amino acid sequences of human MIF and SNCA from the UNIPROT database. In order to construct the 3D models, we compared these sequences with protein sequences with three-dimensional structures deposited in the protein bank (PDB) where several structures of our target proteins have already been subjected. Based on the similarity, we selected our template proteins to build our models, which were two for each protein. The three-dimensional models were created using the Modeller program from the primary structure. The two models chosen for each protein are very similar to each other. For MIF, in the secondary structure analysis of the sequence of each subunit, between 4 and 6 alpha structures and between 3 and 7 beta structures are observed, depending on the analysis program. The models obtained show 4 alpha-helix structures and 5 beta-folded sheet structures, values that are included in those predicted by the programs used. For SNCA, its secondary structure shows two regions with alpha helices and one with beta folding, which matches the predictor and the structure downloaded and seen with pymol. It should be noted that the PYMOL secondary structure recognition algorithms are elementary compared to specialized programs, although the differences were minimal. Therefore, we can assume that they did not affect the possible binding sites with the selected ligand.

When evaluating the models, the Ramachandran graphs were initially analyzed, where most of the residues were found in favorable regions with values between 96% and 98%, while the percentage of residues in unfavorable regions ranged between 0.29% and 0.30%. The model 2 had 5% fewer rotamer outliers than the model 1. Based on this data, both models are of excellent quality. However, for the SNCA models, it was observed that 91% and 88.4% of the amino acid residues were in favorable regions, the latter less than 90% to be considered of excellent quality and with higher values of residues in favorable regions. Compare the two SCNA models with the MIF protein models to see that the SCNA models are of lower quality. The ProSa program, however, calculated a general Z score for the quality of the model, which indicates that the structure of the models is within the range of scores normally found for native proteins of similar size. Since the values were very high, they were close to those obtained for native proteins. The values for SNCA were lower than those of the reference protein,

which suggests that the models are of lower quality when compared to MIF.

With the Verify 3D program, the compatibility of the three-dimensional model with the amino acid sequence was analyzed. Each amino acid is assigned a score ranging from -1 (bad) to +1 (good). For models 1 and 2, approximately 95% of the amino acid residues had a score greater than 0.2, and 100% of the residues had a score greater than 0.2, respectively. The values above zero indicate that the models have 1D-3D compatibility and that the second model is better than the first. For SNCA, the analysis program returned an error, another example of the poor quality of the model.

Next, the models were compared with the template structure and the LDDT score was obtained, which expresses the percentage of interatomic distances present in the template structure that are also conserved in the model, a value of '0' corresponds to zero conserved distances and '1' to a perfect model. In the case of MIF, most of the values were 1 or close to 1, which can be explained by the high degree of similarity between the template and the models. In the case of SNCA, the values were close to zero, which means that the models do not preserve the interatomic distances of the template structure, another evidence of the poor quality of this SNCA model.

The models were analyzed in DoGSiteScorer to see if it could predict cavities on the protein surface where the ligand atoms might be located. Six cavities were detected in both MIF models, one of which yielded a pharmacability score of 0.81. Model 2 had a higher pharmacability than model 1. Drugability is the property of the target protein to have a cavity that allows the union of a small drug-type molecule, according to Lipinskis rules. These rules consist of a series of empirical nature postulates that allow evaluation of how suitable a chemical compound would be to fulfill a pharmacological function once taken as a drug [16].

Considering the results of the analysis of Ramachandran graphs, very3D-1D, and Dogsitescover, the best MIF model corresponded to model 2. This model was chosen to carry out the modeling with the patchdock or DockDoctor tools, which are docking algorithms. A molecule that returns a list of potential complexes formed by the protein and ligands, selected by complementarity of shape. For the molecular docking analysis of SNCA, the decision was made to use a model downloaded from the protein bank, although some

indicators of its quality were not entirely satisfactory.

From the search in the drugbank, several compounds that interacted with the proteins of interest were obtained. However, little pharmacological information is available about these. The first is a compound called 7-Hydroxy-2-Oxo-Chromene-3-Carboxylic Acid Ethyl Ester that binds to the MIF tautomerase active site [17]. The remaining six compounds are being investigated and have antioxidant, anti-inflammatory properties, and affect the immune response, among other things: 3,4-dihydroxycinnamic acid; 4-hydroxyphenylpyruvic acid (ene); 3-(4-hydroxyphenyl)-4,5-dihydro-5-isoxazole-acetic acid methyl ester; 4-hydroxybenzaldehyde o-(cyclohexylcarbonyl)oxime; 3-fluoro-4-hydroxybenzaldehyde o-(cyclohexylcarbonyl)oxime; 4-hydroxybenzaldehyde o-(3,3-dimethylbutanoyl)oxime; 6-hydroxy-1,3-benzothiazole-2-sulfonamide. Only one compound is a drug, and it is also known as ibudilast. Initially developed for the treatment of bronchial asthma, Ibudilast has also been used for cerebrovascular and ocular indications. The drug is a non-selective inhibitor of several phosphodiesterases (PDEs) and has varied anti-inflammatory activity, as well as neuroprotective effects such as NOS inhibition and reduction of reactive oxygen species [18]. Enzymatic analysis shows that these compounds are non-competitive inhibitors of MIF tautomerase activity and interact at the same allosteric binding site of AV411 (ibudilast) and AV1013 (ibudilast analog), findings detected by NMR. Furthermore, experiments with antibodies directed against MIF receptors suggest that CXCR2 is the main target for MIF receptors involved in peripheral blood mononuclear cell chemotaxis [19]. In animal studies, ibudilast significantly reduced alcohol consumption in alcohol-dependent rats and mice. In this way, ibudilast became a possible treatment for alcohol dependence. Ibudilast's utility in treating problematic drinking was demonstrated in human laboratory and preclinical studies. These findings suggest a biobehavioral mechanism through which it works, which reduces the rewarding response to alcohol cues in the brain [18,20].

In the case of SNCA, the drug bank found that the polyphenol resveratrol (3, 5, 4-trihydroxy-trans-stilbene) is the reported active ingredient that interacts with it. Its antioxidant, anti-inflammatory and anti-cancer properties have been reported in vitro, although its activity in vivo has not been

confirmed due to its low bioavailability. Certain mechanisms may be involved, such as activation of EGFR kinase, nuclear factor-kappa B (NFkB), activator protein 1 (AP-1), HIF-1alpha, signal transducer and activator of transcription (STAT3) [21,22]. Cell death is one of the hallmarks of resveratrol. In addition to its neuroprotective effect, it degrades abnormal proteins such as amyloid beta and hyperphosphorylated tau [23]. In this study, alcohol is related to dysbiosis in the organism and dysbiosis with neurodegenerative diseases. Both characteristics are related to alterations in SNCA [24]. Resveratrol has been reported to reduce aggregation and cytotoxicity of SNCA oligomers in animal models, as well as reduce neuroinflammation and oxidative stress. Those findings show that resveratrol may be a good treatment for degenerative diseases and other synucleinopathies as alcoholism [25].

This work evaluated two three-dimensional models for MIF, a downloaded model for SNCA, which yielded reliable results, identifying possible binding sites with drugs or drug candidates and their weak-type interactions.

ABBREVIATIONS

DNA: Deoxyribonucleic Acid
EGFR: Epidermal Growth Factor Receptor
GMQE: Global Model Quality Estimate
IFNGR1: Interferon Gamma Receptor 1
LDDT: Local Distance Difference Test
MIF: macrophage migration inhibitory factor
mRNA: Messenger RNA
NMR: nuclear magnetic resonance
PDB: Protein Data Bank
SNCA: alpha synuclein
SNV: Single-Nucleotide Variant
STAT: Signal Transducer and Activator of Transcription
TNFR1: Tumor Necrosis Factor Receptor Superfamily Member 1A

Declaration of competing interest

None.

Acknowledgments

In part, this work was supported by grants from the National University of Colombia (code Hermes 34766). We must also thank the volunteers who, with their biological samples and participation in filling out forms and questionnaires, made the research possible. They were greatly appreciated. The students and young researchers who worked

hard on projects related to the genetic study of alcoholism in Colombia.

REFERENCES

- [1]. González-Reimers E. Alcoholism: A systemic proinflammatory condition. *World J Gastroenterol* [Internet]. 2014;20(40):14660. Available from: <http://www.wjgnet.com/1007-9327/full/v20/i40/14660.htm>
- [2]. Xiaomin L, Fenglin C, Jianmin H, Yuzhi S, Binsheng G, Yingmei Z. Correlation Between Genetic Polymorphism of Cytokine Genes, Plasma Protein Levels and Bronchial Asthma in the Han People in Northern China. *J Asthma* [Internet]. 2008 Jan 2;45(7):583–9. Available from: <http://www.tandfonline.com/doi/full/10.1080/02770900802032925>
- [3]. Crews FT. Immune function genes, genetics, and the neurobiology of addiction. *Alcohol Res* [Internet]. 2012;34(3):355–61. Available from: <https://www.ncbi.nlm.nih.gov/pmc/articles/PMC3860409/>
- [4]. Crews FT, Lawrimore CJ, Walter TJ, Coleman LG. The role of neuroimmune signaling in alcoholism. *Neuropharmacology* [Internet]. 2017 Aug;122:56–73. Available from: <https://linkinghub.elsevier.com/retrieve/pii/S0028390817300370>
- [5]. Rey Buitrago M. Variantes genéticas, expresión génica, metilación y búsqueda de blancos terapéuticos en vías de respuesta inflamatoria en una muestra de población universitaria colombiana con problemas de consumo de alcohol. Universidad Nacional de Colombia; 2022.
- [6]. Rey M, Aristizabal FA. Inflammatory response genes differentially expressed in a Colombian university cohort with alcohol consumption problems. *Genet Mol Res*. 2023;22(3):1–21.
- [7]. Chaudhuri A, Chant J. Protein-interaction mapping in search of effective drug targets. *BioEssays* [Internet]. 2005 Sep;27(9):958–69. Available from: <https://onlinelibrary.wiley.com/doi/10.1002/bies.20284>
- [8]. Ferreira L, dos Santos R, Oliva G, Andricopulo A. Molecular Docking and Structure-Based Drug Design Strategies. *Molecules* [Internet]. 2015 Jul 22;20(7):13384–421. Available from: <http://www.mdpi.com/1420-3049/20/7/13384>
- [9]. Ai Z, Wang J, Xu Y, Teng Y. Bioinformatics analysis reveals potential candidate drugs for cervical cancer. *J Obstet Gynaecol Res* [Internet]. 2013 May;39(5):1052–8. Available from: <https://onlinelibrary.wiley.com/doi/10.1111/jog.12022>
- [10]. Volkamer A, Kuhn D, Rippmann F, Rarey M. DoGSiteScorer: a web server for automatic binding site prediction, analysis and druggability assessment. *Bioinformatics* [Internet]. 2012 Aug 1;28(15):2074–5. Available from: <https://academic.oup.com/bioinformatics/article/28/15/2074/236684>
- [11]. Jesus FDS, Souza JB De. ANÁLISIS Y CARACTERIZACIÓN DE UNA PROMETEDORA DIANA. *Rev Científica Multidiscip NÚCLEO DO CONHECIMENTO* [Internet]. 2020;9:99–132. Available from: <https://www.nucleodoconhecimento.com.br/salud/objetivo-terapeutico>
- [12]. Altschul SF, Gish W, Miller W, Myers EW, Lipman DJ. Basic local alignment search tool. *J Mol Biol* [Internet]. 1990 Oct;215(3):403–10. Available from: <https://linkinghub.elsevier.com/retrieve/pii/S0022283605803602>
- [13]. Webb B, Sali A. Comparative Protein Structure Modeling Using MODELLER. *Curr Protoc Bioinforma* [Internet]. 2016 Jun 20;54(1):5.6.1–5.6.37. Available from: <https://onlinelibrary.wiley.com/doi/10.1002/cpbi.3>
- [14]. Sun HW, Bernhagen J, Bucala R, Lolis E. Crystal structure at 2.6-Å resolution of human macrophage migration inhibitory factor. *Proc Natl Acad Sci* [Internet]. 1996 May 28;93(11):5191–6. Available from: <https://pnas.org/doi/full/10.1073/pnas.93.11.5191>
- [15]. Vyas N, Companioni RAC, Walfish A, Baum J, Alkhawam H, Tiba M. Association between vitamin D and gastric cancer. *Am J Gastroenterol* [Internet]. 2015;110:S1034. Available from: <http://www.embase.com/search/results?subaction=viewrecord&from=export&id=L72132558%5Cnhttp://dx.doi.org/10.1038/ajg.201>

- 5.281
- [16]. Emamzadeh F. Alpha-synuclein structure, functions, and interactions. *J Res Med Sci* [Internet]. 2016;21(1):29. Available from: <http://www.jmsjournal.net/text.asp?2016/21/1/29/181989>
- [17]. Schrödinger, L., & DeLano W. PyMOL [Internet]. 2020. p. <http://www.pymol.org/pymol>. Available from: <http://www.pymol.org/pymol>
- [18]. Lipinski CA. Rule of five in 2015 and beyond: Target and ligand structural limitations, ligand chemistry structure and drug discovery project decisions. *Adv Drug Deliv Rev* [Internet]. 2016;101:34–41. Available from: <http://dx.doi.org/10.1016/j.addr.2016.04.029>
- [19]. Orita M, Yamamoto S, Katayama N, Aoki M, Takayama K, Yamagiwa Y, et al. Coumarin and Chromen-4-one Analogues as Tautomerase Inhibitors of Macrophage Migration Inhibitory Factor: Discovery and X-ray Crystallography. *J Med Chem* [Internet]. 2001 Feb 1;44(4):540–7. Available from: <https://pubs.acs.org/doi/10.1021/jm000386o>
- [20]. Bell RL, Lopez MF, Cui C, Egli M, Johnson KW, Franklin KM, et al. Ibudilast reduces alcohol drinking in multiple animal models of alcohol dependence. *Addict Biol* [Internet]. 2015 Jan;20(1):38–42. Available from: <https://onlinelibrary.wiley.com/doi/10.1111/adb.12106>
- [21]. Cho Y, Crichlow G V., Vermeire JJ, Leng L, Du X, Hodsdon ME, et al. Allosteric inhibition of macrophage migration inhibitory factor revealed by ibudilast. *Proc Natl Acad Sci* [Internet]. 2010 Jun 22;107(25):11313–8. Available from: <https://pnas.org/doi/full/10.1073/pnas.1002716107>
- [22]. Grodin EN, Bujarski S, Towns B, Burnette E, Nieto S, Lim A, et al. Ibudilast, a neuroimmune modulator, reduces heavy drinking and alcohol cue-elicited neural activation: a randomized trial. *Transl Psychiatry* [Internet]. 2021;11(1):1–8. Available from: <http://dx.doi.org/10.1038/s41398-021-01478-5>
- [23]. Gambini J, López-Grueso R, Olaso-González G, Inglés M, Abdelazid K, El Alami M, et al. Resveratrol: distribución, propiedades y perspectivas. *Rev Esp Geriatr Gerontol* [Internet]. 2013 Mar;48(2):79–88. Available from: <https://linkinghub.elsevier.com/retrieve/pii/S0211139X12001023>
- [24]. Shakibaei M, Harikumar KB, Aggarwal BB. Resveratrol addiction: To die or not to die. *Mol Nutr Food Res* [Internet]. 2009 Jan;53(1):115–28. Available from: <https://onlinelibrary.wiley.com/doi/10.1002/mnfr.200800148>
- [25]. Corpas R, Grinán-Ferré C, Rodríguez-Farré E, Pallàs M, Sanfeliu C. Resveratrol Induces Brain Resilience Against Alzheimer Neurodegeneration Through Proteostasis Enhancement. *Mol Neurobiol* [Internet]. 2019 Feb 13;56(2):1502–16. Available from: <http://link.springer.com/10.1007/s12035-018-1157-y>
- [26]. Liu X, Vigorito M, Huang W, Khan MAS, Chang SL. The Impact of Alcohol-Induced Dysbiosis on Diseases and Disorders of the Central Nervous System. *J Neuroimmune Pharmacol* [Internet]. 2022 Jun 29;17(1–2):131–51. Available from: <https://link.springer.com/10.1007/s11481-021-10033-4>
- [27]. Zhang L, Yu X, Ji M, Liu S, Wu X, Wang Y, et al. Resveratrol alleviates motor and cognitive deficits and neuropathology in the A53T α -synuclein mouse model of Parkinson's disease. *Food Funct* [Internet]. 2018;9(12):6414–26. Available from: <http://xlink.rsc.org/?DOI=C8FO00964C>